Sub-millisecond switching of multi-level liquid crystal on silicon spatial light modulators for increased information bandwidth

MIKE PIVNENKO, [1] KUN LI, [1,2] AND DAPING CHU [1 *]

[1] *Centre for Photonic Devices and Sensors, University of Cambridge, 9 JJ Thomson Avenue, Cambridge, CB3 0FA, UK*
[2] *Display R&D Center, Southeast University, Nanjing, Jiangsu, China*
** Corresponding author: dpc31@cam.ac.uk*

Abstract: Sub-millisecond response time with a refresh rate higher than 2000 frames per second (fps) and no degradation of the contrast ratio or diffraction efficiency is demonstrated in working liquid crystal on silicon (LCOS) spatial light modulators (SLMs) with 8-bit grey levels of amplitude and phase modulations. This makes possible to achieve an information bandwidth of about 190 Gb s^{-1} with a 4k LCOS operating at 10-bit phase modulation levels. The normalised contrast stays at almost the unit level for a frame rate up to 1700 fps and at higher than 0.9 for 2500 fps. The diffraction efficiency stays above -1.0 dB for a frame rate up to 2400 fps. Such a fast response allows to eliminate image blurring in replaying a fast movie.

1. Introduction

Spatial Light Modulators (SLM) have seen its applications widely spread in many different industries, including displays [1–6], laser processing [7,8], optical-tweezers [9,10], telecommunications [11–14] over the past twenty years. Two competing technologies are mostly used for the SLMs, Digital Micromirror Devices (DMDs) and Liquid Crystal on Silicon (LCOS) devices. DMDs have a fast switching speed [15,16], but they can only be used for amplitude modulations and the diffraction efficiency is limited due to a conjugate image due to its binary nature. LCOS devices can be used for both amplitude and phase modulations [17][18] and can achieve multi-grey-level phase-only modulations, but the most challenging aspect in LCOS SLM is the switching speed [19–22].

Slow switching LCOS SLMs result in a limited information bandwidth and breakups in colour sequential operations [23,24], also they cannot be used in tiling arrangements, often adopted by DMDs [25], to enlarge field of view or viewing angle. Faster LCOS need to be developed to match the development of video rate hologram generation [26] and for using LCOS in OAM coding/decoding [27]. Various liquid crystal (LC) mixtures, electrode structures and driving scheme have been demonstrated to reduce the switching time to a few and even sub-milliseconds [28–35], but much of them are either for the amplitude modulation or demonstrated only in glass testing cells.

For phase modulation, high birefringent or large dielectric anisotropy LCs have been developed [36]. These materials are often used with a polymer network for a faster response time [37–39]. However, the driving voltages are high because of the polymer existence [40]. A mixture of an LC and a polymer has increased light scattering for the visible wavelength and therefor usually used for IR applications. For blue phase LCs, although the response time for both the rise and decay processes is in the range of 100 μs, the high electric voltage is not suitable for the LCOS operation [41,42]. Ferroelectric LC or chiral smectic LC are used in LCOS to modulate phase and can achieve two orders of magnitude faster switching speed than conventional nematic devices [43,44]. Unfortunately, the binary phase operation results in a significant loss of incident light to symmetric diffraction orders [45].

Nematic LC mixtures are still the most practical ones to use for continuous phase depth modulations in LCOS SLMs, they are reliable and only require a few volts to reach 2π phase modulation. Recently, a considerable reduction of the phase flicker due to digital modulation was demonstrated and 10-bit phase modulation was realized [46,47]. Most recently, high birefringent nematic LC mixtures are reported to achieve a 8.32 ms average phase-to-phase response time at 40°C in transmissive homogenous glass cells, nevertheless the equivalent response time in LCOS is extrapolated, not demonstrated [48]. However, there is a fundamental difference between the glass test cells and LCOS devices, because of the fringe field [49] and cross-talk between adjacent pixels, which makes the diffraction efficiency can only be quantified using actual LCOS devices.

In this paper, we demonstrate fast response time in working LCOS SLMs with 8-bit grey level amplitude and phase modulation for the visible wavelength range applications. The same LCOS SLM was modulated for phase-only applications and amplitude applications separately. For phase-only applications, the LCOS can achieve more than 2π of phase depth modulation at 640nm wavelength. Sub-millisecond response time and refresh rate higher than 2000 frames per second (fps) with no degradation of the contrast ratio or diffraction efficiency is demonstrated. This makes a bandwidth about 190 Gb s^{-1} potentially achievable for a 4K LCOS with 10-bit modulation: (~ 4×10^3 pixels × 2.4×10^3 pixels × 2000Hz × 10 bits) comparing to currently available full high definition LCOS device with a bandwidth about 2.9 Gb s^{-1} (2×10^3 pixels × 10^3 pixels × 60Hz × 3 colures × 8 bits). Fast video clips (240 Hz) are loaded to both fast and normal LCOS to demonstrate the enhanced switching effects.

2. LCOS response time

LCOS SLMs working in anti-parallel aligned Electrically Controlled Birefringence (ECB) mode utilise a positive dielectric nematic LC, which usually has a larger magnitude of dielectric anisotropy than the negative dielectric nematic LC used in the Vertical Aligned (VA) LCOS SLMs. As a result, the VA LCOS SLMs has a higher threshold voltage and a slower response time [22]. In this paper, we will focus on LCOS SLMs with the positive dielectric nematic LC in the anti-parallel aligned ECB mode.

The LCOS response time mainly consists of the LC switch-on time (t_{on}) and the LC switch-off time (t_{off}). The t_{off} is effectively the intrinsic LC relaxation time when the driving voltage is removed, hence it is usually a few times longer than t_{on} which relies on the driving voltage. Therefore, reducing the t_{off} is essential, and the most effective way is reducing the LC layer thickness, because the t_{off} is proportional to the square of LC thickness,

$$t_{off} = \frac{\gamma_1 d^2}{K_{11}\pi^2}, \quad (1)$$

Where γ_1 is the LC rotational viscosity, d is the LC thickness, K_{11} is the LC splay elastic constant. The minimum LC thickness (d_{min}) is determined by the target phase depth (δ_{min}) and LC birefringence (Δn) at the designed wavelength (λ) by the equation

$$d_{LCoS} = \frac{d_{min}}{2} = \frac{\delta_{min} \times \lambda}{2 \times 2\pi\Delta n}, \quad (2)$$

whereas d_{LCoS} is the minimum LC layer thickness in LCOS SLMs and it is a half of the d_{min}, taking into account double light pass in a reflective device.

2.1 LC properties

In this study, we selected high birefringence nematic LC MDA-98-1602 (Merck KGaA) with the Δn of 0.25 at 650 nm, 20C and clearing temperature 109C. The birefringence of this LC was measured for the visible range of the wavelength, 400-700nm, and temperature from 24 to 100C, Figure 1. The measurements were done by observing transmission spectra (Spectrometer USB4000, Ocean Optics) of an LC cell between crossed polarisers. The experimental data points were fit with the extended Cauchy model [50], shown as continues lines on Figure 1a. At 60C the birefringence at 650nm goes down to 0.22 and this value was used to calculate the

required cell thickness to guaranty 2π phase depth for the full range of the working wavelength and temperature.

Although the high birefringence LC can reduce the d_{min}, other LC properties like viscosity, splay elastic constant and material stability need to be taken into account while selecting the best candidate. Visco-elastic ratio $\frac{\gamma_1}{K_{11}}$ for this LC was measured [47] for a range of temperatures, the value was about 15 ms/μm^2 at 20C and decreased to 5 ms/μm^2 at 60C, which offers a short t_{off} according to Equation (1).

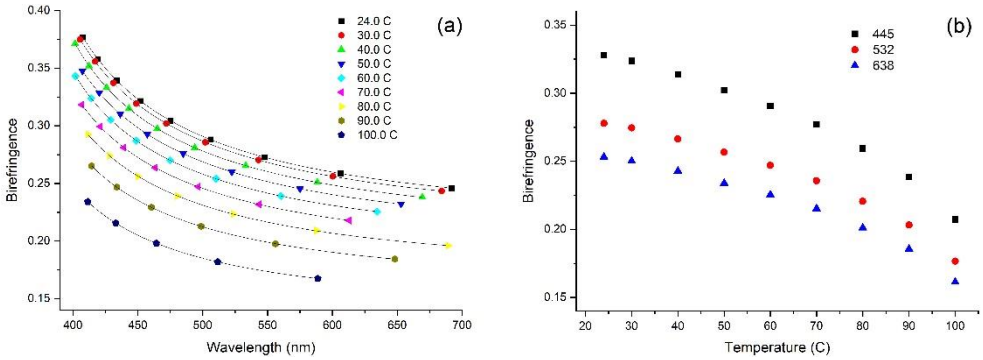

Fig. 1. Birefringence of nematic LC MDA-98-1602 as function of (a) wavelength and (b) temperature.

Using fast LC with short response time and digital pulse-width modulation driving can lead to elevated level of the phase flicker, which could be a problem for the amplitude modulation and particularly for the phase modulation. Careful selection of the driving pattern and phase flicker optimisation has to be done. A deep learning model optimisation technique [47] applied for an LCOS with this fast LC allows reduction of the flicker to so low the level that 10-bit modulation is possible. However, in this paper we limited to 8-bit to pay more attention to other properties.

2.2 Test cells and methodology

The selected LC material is made into transmissive glass test cells to evaluate its switching response in the ECB mode, especially under the various driving voltages and working temperatures. Using the Equation (2), the theoretical d_{min} that can achieve 1π phase depth in transmissive cells and 2π phase depth in reflective LCOS devices is calculated to be 1.3 μm. However, this d_{min} is based on the infinite driving voltage at 20°C operational temperature, which is not the case with real LC cells and LCOS SLMs. In practice, the maximum voltage range in LCOS driver board is limited to 3-5 Vrms, and the operational temperature regularly increased to 35-40 °C and can reach 60C. As a result, the LC birefringence and the maximum phase depth of LCOS would decrease. In addition, the die assembly process used in our study often introduces a small uncertainty in the LC layer thickness and performance due to substrates not being perfectly flat and a physical rubbing procedure. Taking all considerations into account, the LC test cells are assembled with a thicker LC layer of 2 μm to guarantee the target phase depth.

The test cells are driven with electric signals of a square wave shape at 1 kHz frequency from a signal generator Tektronix AFG31000. The phase modulation process of test cells is observed with a microscope Olympus BX53. When the cell is placed between cross polarisers, at a 45° angle with respect to the polarisation direction of both polarisers, the intensity of transmitted light changes as a result of the LC phase modulation. The intensity change is measured by a photodiode Thorlabs PDA100A while driving voltages are scanned between 0 and 5V rms. The driving voltages that result in the minimum (I_{min}) and maximum (I_{max})

intensities are set as the V_B and V_W respectively, subscript 'B' denotes black and 'W' denotes white. The difference between the I_{max} and I_{min} is ΔI.

The transition time interval which the intensity changes from 90% to 10% of ΔI is the t_{on}, and the reverse is t_{off}, Figure 2(a) and (b). Such measurements are repeated at different temperatures between 25-65 °C and results are plotted in Figure 2(c), where the temperature of the test cell is controlled by a heating and freezing microscope stage (THMS600, Linkam Scientific Instruments, Surrey, UK). During the measurement process, the LC Δn reduces slightly as the temperature increases, the voltages are adjusted to ensure that the I_{min} and I_{max} are always achieved and the 1π of phase modulation is not changed. The adjustment is small, within 10% of the V_B and V_W.

As shown in Figure 2(c), both the t_{on} and t_{off} decreases with the increasing temperature between 25-65 °C, from 0.8-0.3 ms and from 2.1-0.9 ms respectively. This is expected as the viscosity of the LC material reduces with temperature which results in an increased response. The t_{on} is several times smaller than the t_{off} at each temperature. The overall switching cycle t_{on+off} is just below 3ms at 25 °C, corresponding to switching frequency of over 330 Hz, it reduces to just over 1 ms (close to 1000 Hz frequency) at 65 °C. With a fixed LC layer thickness, increasing temperature is very effective in reducing the LC switching time further.

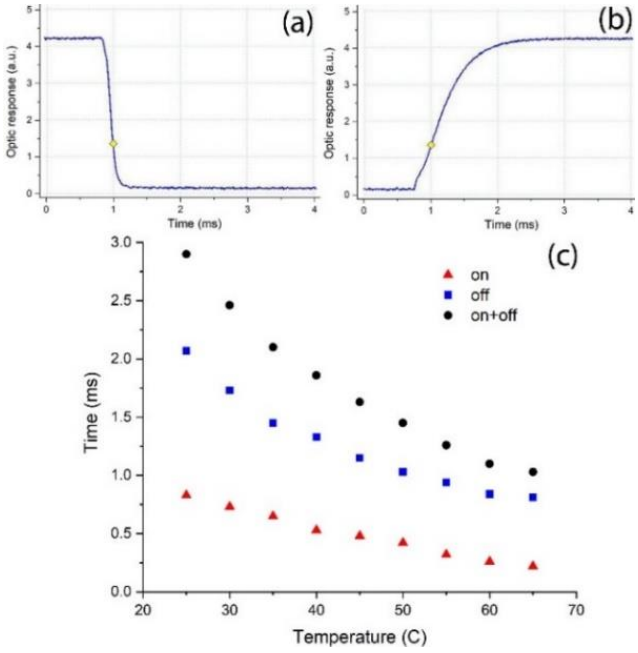

Fig. 2. Optic responses for (a) voltage on and (b) voltage off, and (c) the response time of a 2 μm LC transmissive test cell, with a 1π phase modulation measured at 640 nm and temperature range of 25-65 °C.

The glass test cells have been driven with an analogue scheme and fixed frequency waveform while the rms voltage varies. On the other hand, LCOS SLM is driven with a digital pulse-width modulation driving scheme where equivalent rms voltage achieved by changing the waveform and modulating the pulse width.

2.3 LCOS preparation

The LCOS SLMs are assembled in the Class 100/1000 cleanroom in house [51], and they are based on digital-driving Si backplanes from Jasper Display Corp. A polyimide alignment layer is spin coated and rubbed to provide initial alignment directions for LC to work in the ECB

mode. The LCOS SLM have a 2 μm thick LC layer, and it has a minimum phase depth of 2π for a phase-only modulation, at the same time it can be used for amplitude modulation while modulating within 1π phase depth.

The Si backplane has a resolution of 1920x1080 pixels and a pixel pitch of 6.4 μm. An ASIC driving board (SRK JD7554, Jasper Display Corp.) is used, which provides a maximum of 5.0 V rms driving voltage and is configured to run a sequential row-by-row scanning driving scheme. Digital pulse-width modulation was used to achieve 8-bit grey scale resolution. The limitation of the bandwidth of HDMI video interface between a PC and the driver lead to a limit of what frame rate can be sent from a PC to the LCOS. As a result, the refresh rate of 60 Hz can be achieved when scanning all 1080 rows of pixels with 8-bit grey level resolution, 120 Hz when scanning 540 rows, 240 Hz when scanning 270 rows and 480 Hz when scanning 135 rows, as shown in Figure 3(a) to 3(d) respectively. The frame rate can be further increased but the active rows are too few and the operating system interface cannot be displayed to carry out the test.

The parallel interface between the driver and the LCOS allows much higher frame rate to be tested. In his paper we used frame rate up to 4000fps, 8-bit grey level resolution, which was enough to reach and test the LC response time limit. But this also means that the content has to be generated in the driver or be preloaded to the driver memory which limits the content variety.

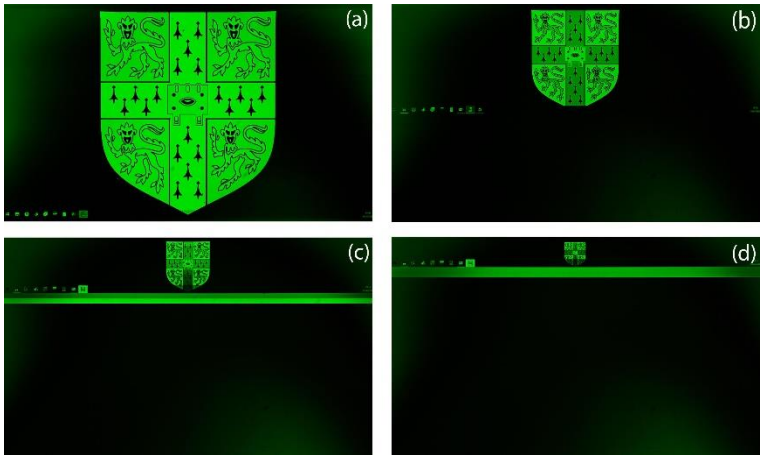

Fig. 3. Images (University of Cambridge Crest) shown on the LCOS device when the driving board is scanning (a) 1080 rows at 60 Hz, (b) 540 rows at 120 Hz, (c) 270 rows at 240 Hz, or (d) 135 rows at 480 Hz.

2.4 Voltage adjustment method

Accurate adjustment of the driving voltage allows considerable improvement of the refresh rate. This section describes how to determine the required range of the driving voltages in use for different phase modulation depths at different switching speeds.

Figure 4 schematically shows typical variation of the phase modulation by an LCOS device as a function of driving voltage. The phase as a function of voltage

$$\varphi = \mathrm{F(V)} \tag{3}$$

depends on the selected LC and pulse-width modulation driving protocol. This function was measured experimentally and used to find required driving voltage for particular values of the phase. The driving voltages are set as the V_B and V_W, subscript 'B' denotes black and 'W' denotes white frame. Required phase depth φ_0 depends on the application, for example π radians for amplitude modulation or phase modulation with binary grating, or 2π for phase modulation with blazed grating and holography. Usually, V_B is set just a bit higher than the threshold voltage V_{th} and V_W is set to get the required phase depth φ_0. However, considerable

improvement of the response time is achieved if driving voltage is set to a higher values – V'_B and V'_W, providing that the required phase depth φ_0 is maintained. The effect of increasing driving voltage on the response time is shown on Figure 5.

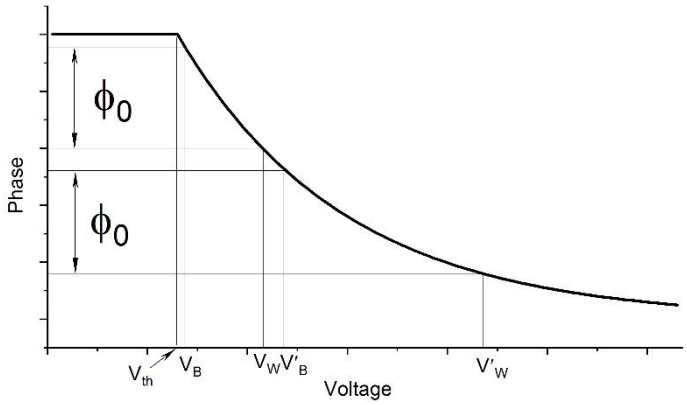

Fig. 4. Schematic typical dependence of the phase modulation on driving voltage.

Figure 5 shows how response time of an LCOS device can be reduced by increasing driving voltage V_B from 0.8 to 2.2V. Driving voltage V_W was set in a range from 2.5 to 5.0V, accordingly, to keep the phase depth φ_0 equal π radians for amplitude modulation. Driving voltage V_W was about 1.7 to 2.8V higher than V_B. At the low driving voltage setting the total response time, which is a sum of the fall time and rise time, is about 5 ms and corresponds to a refresh rate of 200 fps. At the high voltage setting, total response time is about 1.2 ms and corresponds to a refresh rate of 800 fps. In this case the driving voltage V_B and V_W set fixed at low refresh rate and does not change with the refresh rate.

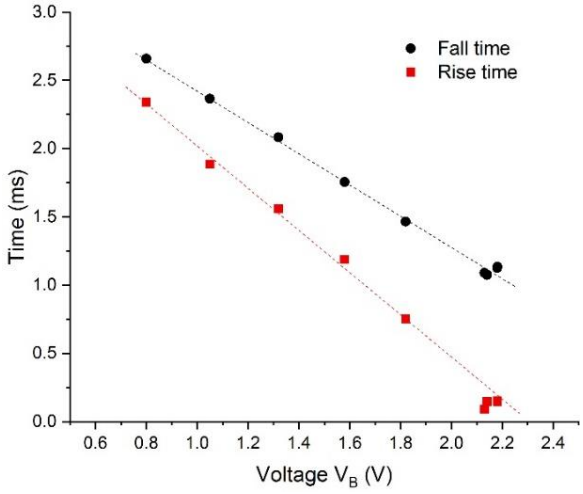

Fig. 5. LCOS response time as function of V_B driving voltage.

In order to minimise the total response time, driving voltage V_W was set to the highest available (for the driver) value and then driving voltage V_B adjusted to get required modulation phase depth φ_0, the value of π of 2π for amplitude and phase modulation, respectively. This adjustment of the V_B voltage has to be repeated for higher frame rate in order to keep the required value of the phase. Figure 6 explains how this is done.

Figure 6(a) shows schematic of the phase variation over time for an LCOS device with low refresh rate (long period). The period is long enough for the phase to reach saturation, both on

increase and decrease of the phase, and to achieve the required phase depth φ_0. With a higher frame rate (shorter period) the phase saturation cannot be achieved and total phase depth φ_1 becomes lower than required φ_0, Figure 6(b). However, by adjusting driving voltage V_B to a new value V_B', the phase depth can be increased back to the original φ_0 level, Figure 6c. Figure 7 explains how the new value V_B' is calculated.

To minimise the response time for a particular refresh rate, driving voltage V_W was set to the highest available (for the driver) value and then voltage V_B' adjusted to get the required modulation phase depth φ_0 (π or 2π), now at the given increased refresh rate. The new value of the driving voltage V_B' for a particular refresh rate can be numerically calculated from the experimental function (3) of the phase modulation of driving voltage with the following equation:

$$\varphi_2 = F(V_B'), \tag{4}$$

where the value of phase φ_2 can be calculated from the required phase value φ_0 and the measured φ_1 through a linear relationship: $\varphi_2 = \varphi_0 \frac{\varphi_0}{\varphi_1}$. Linearisation is justified here because the changes of the variables are relatively small.

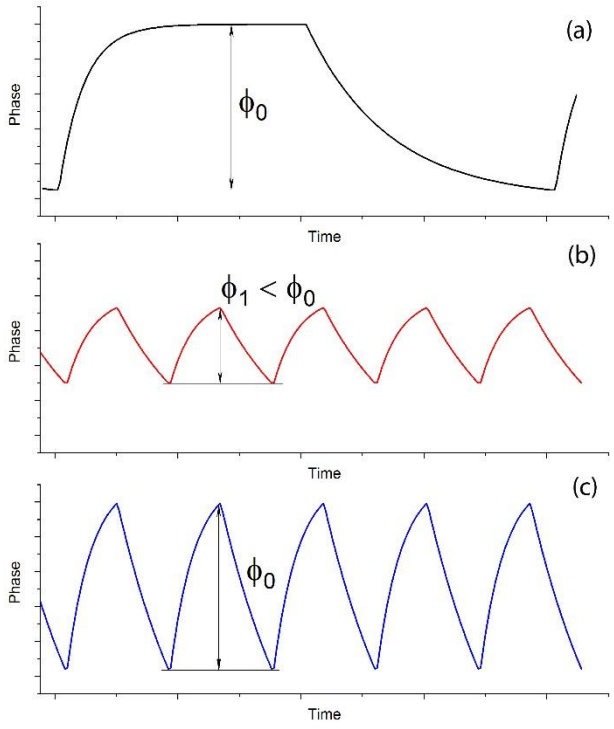

Fig. 6. Phase variation over time for LCOS device with (a) low refresh rate, (b) high refresh rate and fixed driving voltage, and (c) high refresh rate and adjusted driving voltage.

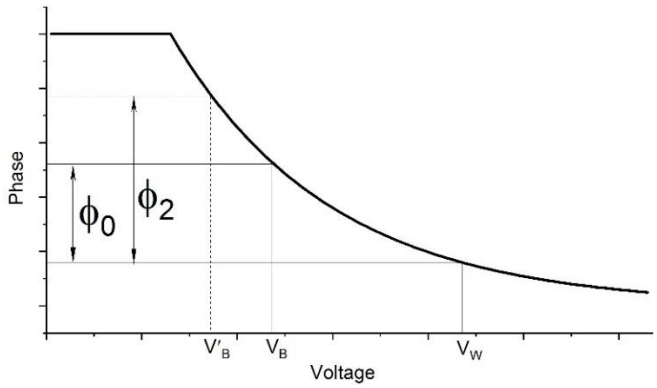

Fig. 7. Driving voltage adjustment for high refresh rate.

Figure 8 shows an example of driving voltage V_B' adjustment and corresponding improvement of the refresh rate. An image of a binary diffraction grating with grating period of 16 pixels was applied to an LCOS device. Driving voltage V_W was set to value 5V, the highest available for the driver, and driving voltage V_B = 2.48 V was calculated from Eq. 3 to get modulation phase depth $\varphi_0 = \pi$ required to maximise diffraction efficiency for binary grating. Diffraction pattern for green light of 532 nm was observed and power of the first diffraction order was measured for low refresh rate of 50 fps and used as a reference. The power of the first diffraction order for fixed driving voltage was measured for the refresh rate in the range from 100 to 3500 fps and normalised on the reference value, Figure 7 (black dots). It shows continuous decrease for refresh rate higher than 700 fps. In order to test the voltage adjustment, for every refresh rates in the range from 100 to 3500 fps, the adjusted driving voltage V_B' was calculated according to Equation (4), Figure 7 (triangles). The power of the first diffraction order for the adjusted driving voltage was also measured and normalised on the reference value, Figure 8 (squares). As a result, the refresh rate considerably improved. For example, for the normalised diffraction efficiency of 0.95, maximum refresh rate increased from 850 to 2150 fps due to the voltage adjustment.

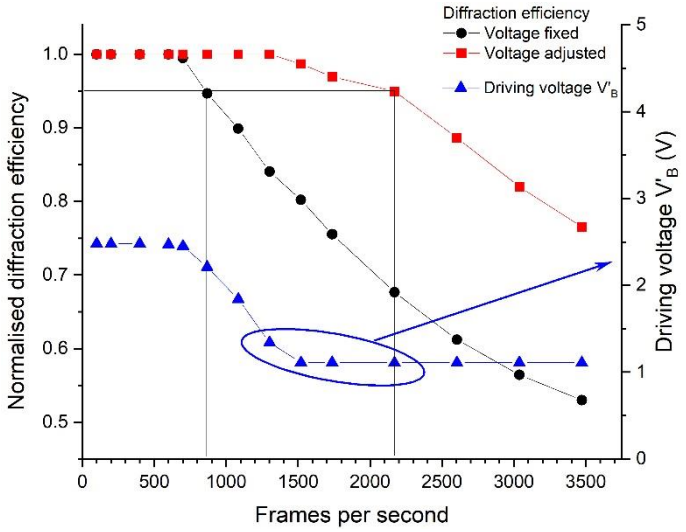

Fig. 8. Normalised diffraction efficiency of a binary grating for different refresh rates. For fixed voltage setting V_W = 5.0V, V_B = 2.48V. For adjusted voltage setting V_W = 5.0V, V'_B is blue triangles on the graph.

3. Imaging with high refresh rate

To demonstrate how an LCOS device with fast responding liquid crystal can improve blur reduction for high frame rates we observed a movie with a fast moving image. In a movie with 240 fps refresh rate an image was moving across a frame with velocity 3840 pixels per second. For a typical 24 inch monitor (1920x1200) with viewing distance of 20 inches this corresponds angular speed of about 100 degree per second. A snapshot was taken with 100 μs exposure time to eliminate any blur from the exposure. Figure 9 shows the results for a fast LCOS device described in this paper and a reference LCOS device. As a reference a commercially available LCOS device with specified response time of 30 ms was used. Due to slow liquid crystal response in the reference device a long trail is observed after an image corresponding to the response time about 30 ms. The fast LCOS with response time about 700 μs shows no image blur. The reference LCOS also shows reduced level of image contrast due to long trails from any objects of the scene. The trail is so long that it is still visible to the right of the tower from the previous frame.

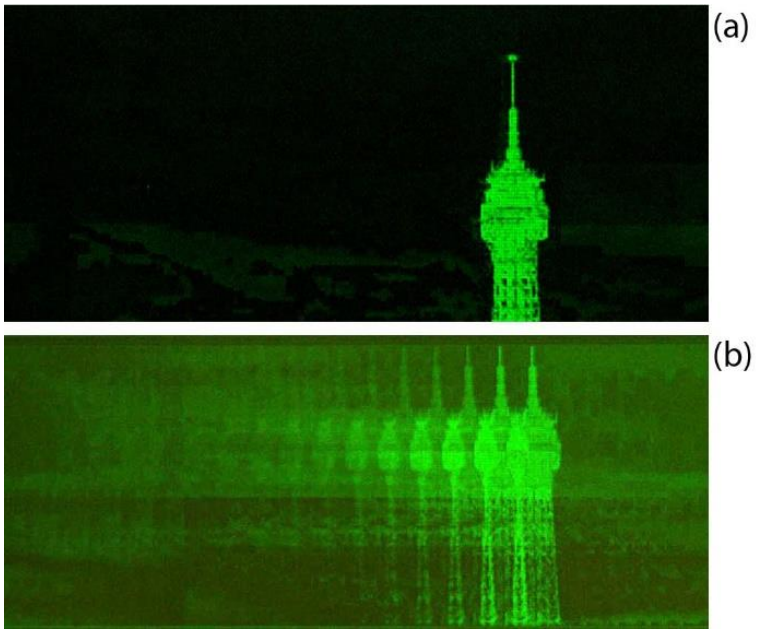

Fig. 9. Blur reduction of a fast moving image on (a) a fast LCOS with a response time of ~700 μs in comparison to that on (b) a reference LCOS device with a response time of ~30 ms.

The image contrast was also tested with a fast LCOS device in the amplitude mode with phase depth of 1π radian. A continuous sequence of black and white frames was applied and brightness was measured as a function of time. The absolute value of the contract ratio depends on the light leakage in the dark state. With proper optimisation and use of phase compensators the value can reach a few thousands. Such optimisation is beyond the scope of this paper, we observed the value of about 300. The aim was to see how the image contrast goes down when the LC reaches its response time limit. The maximum contrast between the brightness of the white and black frames at low frame rate of 50 fps was set as a unit reference. Figure 10 shows the waveform for the four examples with the result for the frame rates from 500 to 2610 fps.

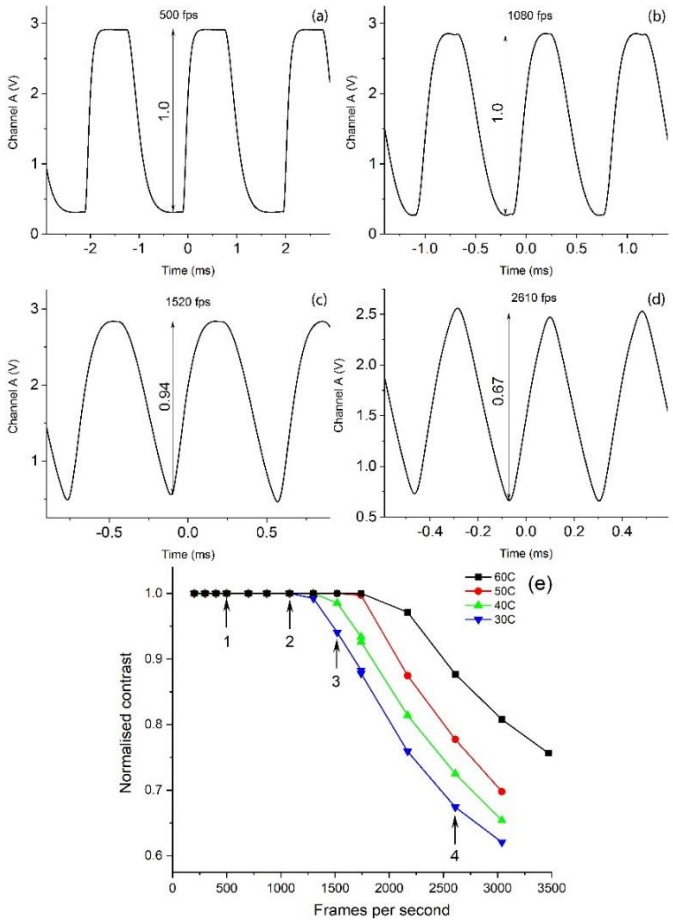

Fig. 10. Image contrast as a function of the refresh rate, (a) 500 fps, (b) 1080 fps, (c) 1520 fps and (d) 2610 fps, and (e) temperature.

The shape changes from rectangular for low frame rates to sin-like for higher frame rate when LC becomes too slow to include the higher harmonics of the signal. At 30 °C the normalised contrast stays higher than 0.94 for the frame rates up to 1520 fps and higher than 0.67 for the frame rates up to 2610 fps. Figure 9 also shows how the contrast changes with increasing frame rate for higher temperatures from 30 to 60 °C. At 60 °C the normalised contrast stays at almost the unit level for frame rate up to 1700 fps and higher than 0.9 for 2500 fps.

4. Fast switching of 8-bit multilevel image

To verify how fast the LCOS can switch for an 8-bit multilevel image, we did the following experiment. A continuous sequence of images of a linear ramp blazed phase grating with 8-bit grey level resolution and 32 pixel pitch, switching from frame to frame between horizontal and vertical orientations, was applied to the LCOS panel. The LCOS was observed between crossed polarisers at 543 nm with a fast camera (Zyla 5.5, Andor). With the frame size of the camera limited to 64 by 256 pixels and global shutter, the camera can reach 1230 fps; the exposure time was set to 0.4 ms. Figures 11(a) and (b) show two consecutive frames with a separation of 0.813 ms. The grating is fully switched from the vertical to horizontal state, which means that 0.413 ms (the difference between the frame time and the exposure time) was enough to finish all the transient switching of the multilevel image.

To improve the time and spatial resolutions of the image, a stroboscopic illumination was used. We used a high power LED light source modulated by an external driver (SOLIS-525C with DC2200 driver, Thorlabs) which is synchronised with the LCOS frames. A signal generator with controllable time delays (AFG31021, Tektronix) allowed to set the illumination flashes to a particular part of the frame. The LCOS was switching with 1403 fps rate, 0.713 ms per frame, and an image of a blazed grating with 128 pixel pitch and switching orientation was applied. The illumination time was set to 0.400 ms and tuned to the middle of the frame with the vertical grating shown in Fig. 11(c), or that with the horizontal grating shown in Fig. 11(d). The grating can be regarded as fully switched from one state to another in 0.313 ms of time, with only some residuals of high contrast edges of the previous frame which are barely visible. Higher refresh rates are also possible by reducing the illumination time with a reasonable limit of about 1600 fps when the illumination time and switching time are equal.

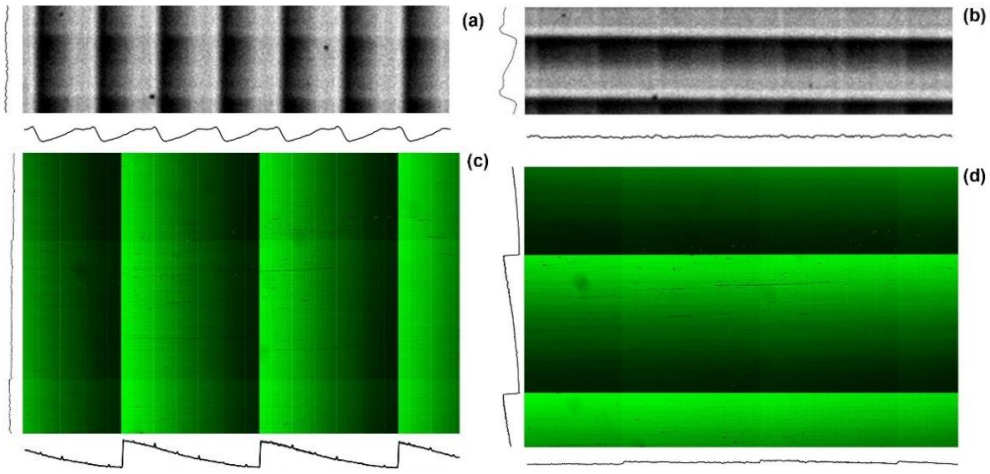

Fig. 11. Two consecutive frames, (a) and (b), with 0.813 ms separation taken with a fast camera and two consecutive frames, (c) and (d), with 0.713 ms separation taken with a stroboscopic illumination. The LCOS was set at the frame rates of 1230 fps and 1403 fps, respectively, with V_B = 0.397 V, V_W = 4.960 V, and T = 60 °C.

5. Diffraction efficiency with pitches down to single pixel level

The diffraction efficiency reduction due to higher refresh rate was tested for a fast LCOS device on diffraction for green light of 532 nm. An image of a binary diffraction grating with the pitch of 16 pixels, stripes of 8 pixel wide with phase depth of 0 and π radians, was applied and the power of the first diffraction order was measured for a range of frame rates and temperatures. A frame with the grating and a frame with no grating, uniform phase level, were switched sequentially. We observed how the power of the first diffraction order goes down for higher frame rate due to degradation of the grating quality for the LC response limitation. Power of the first diffraction order measured for low frame rate of 100 fps was set as a reference, 0dB. Figure 12 shows what frame rate can be achieved for a fixed reduction of the diffraction efficiency between -0.1 and -3.0 dB for different temperatures. For example, at 60 °C fast frame rate does not influence the diffraction efficiency more than -1.0 dB for frame rate up to 2400 fps.

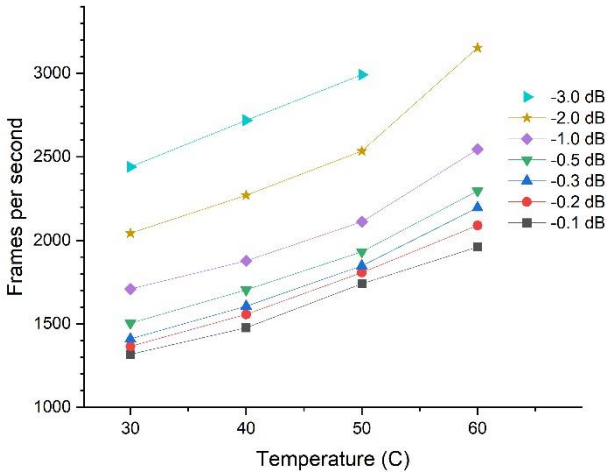

Fig. 12. Diffraction efficiency loss due to high refresh rate as a function of temperature.

Switching LC as a full frame, when all the pixels move uniformly, is very different from switching every pixel individually. When neighboring pixels are at different state the fringe field and cross-talk between adjacent pixels reduces diffraction efficiency. To analyse how higher spatial frequency may influence diffraction efficiency at high frame rates, diffraction on gratings with different grating pitch was measured. Diffraction gratings with the pitch decreased from 512 pixels to 2 pixels, horizontal (along rubbing direction), vertical and "checkerboard" was applied to a fast LCOS device and intensity of the first order diffraction was measured and normalized on its level for low frame rate. As shown in Figure 13, the diffraction efficiency for 700 fps stays at its maximum level with the grating pith reduced from 512 to 16 pixels and only then goes down. For the grating pitch of two pixels, this means only one pixel switches surrounded by two unswitched pixels (or four for the "checkerboard" grating) the diffraction efficiency is about 0.85 of its maximum level. The result does not depend much on whether the grating is horizontal, vertical or "checkerboard". For a higher refresh rate of 1300 fps vertical and "checkerboard" gratings show faster decrease at high spatial frequencies. This is due to specific defects appearing on the right side of vertical stripes. The defects observed at higher driving voltages are required for fast refresh rates. The origin of these defects is outside of the scope of this paper and will be described elsewhere.

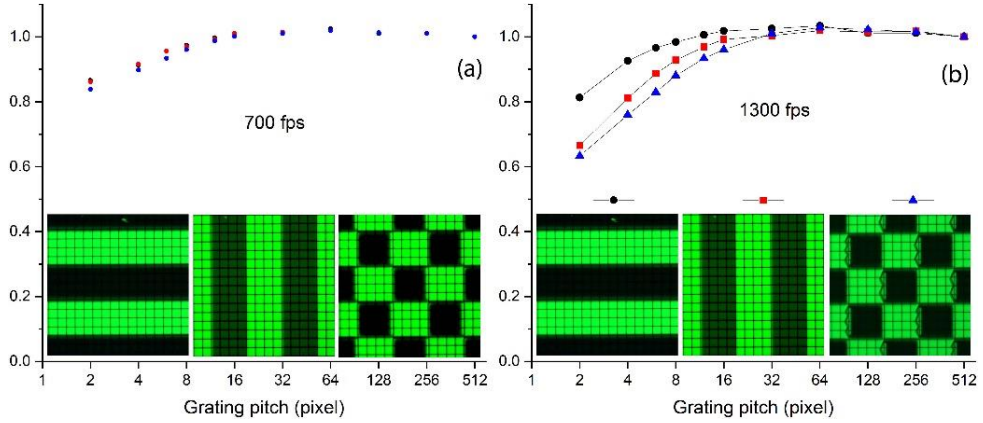

Fig. 13. Normalised diffraction efficiency as a function of the grating pitch at different refreshing rates, (a) 700 fps and (b) 1300 fps.

6. Discussions and conclusions

It is worth to point out that there are two important aspects which are both essential for getting a fast response time and managing a high refresh rate, namely a suitable LC material with the right layer thickness and an appropriate driving scheme.

Our work demonstrates how to get these two aspects working together. The key points and the novelty of this work can be summarised in the following:

1. A suitable nematic LC material was selected based on its high birefringence and low visco-elastic ratio, allowing the reductions of the device thickness and response time. This LC material was tested in both a standard single pixel glass LC cell and a working LCOS device for the full working range of the visible wavelength and temperature.
2. An appropriate driving voltage adjustment was applied for digital pulse-width modulation schemes, and a significant improvement of the response by a factor of 5 to 20 was achieved depending on the driving condition in use.
3. The benefit of the reduced response time was translated into the technical characteristics of LCOS devices suitable for both amplitude and phase modulations. The results are presented in a form similar to that of the Modulation Transfer Function (MTF) which is widely used by optical engineers. This allows a user to select the required balance between a fast response and high image quality or diffraction efficiency.
4. Fast response times at the kHz level was demonstrated in a working 8-bit grey scale LCOS device. This allowed the measurement of the actual diffraction efficiencies and the test of how the field fringe effect between adjacent pixels influencing the diffraction performance in a phase-only LCOS SLM when the response time was pushed to a limit, which are not possible with a standard single pixel glass LC cell of a high response time.

In conclusion, fast sub-millisecond response in working multi-level LCOS SLMs with 8-bit grey levels of phase resolution is demonstrated for the visible wavelength range. Refresh rates higher than 2000 fps with no degradation of the contrast ratio or diffraction efficiency are realised. Such a high refresh rate will enable a wide range of applications, e.g. three-colour and two-time sequential for full colour stereoscopic video displays based on a single LCOS panel. It also makes possible to achieve an information bandwidth of about 190 Gb s^{-1} with a 4K LCOS operating at 10-bit phase modulation. Driving voltage adjustments allow to keep the LCOS response flat for high refresh rates. For the normalised diffraction efficiency of 0.95, the maximum refresh rate can be increased from 850 to 2150 fps through driving voltage adjustments. Temperature dependence of the LCOS response is also analysed. For 60 °C the normalised contrast stays at almost the unit level for frame rates up to 1700 fps and higher than 0.9 for 2500 fps. Operating at fast frame rates up to 2400 fps affects the diffraction efficiency for less than -1.0 dB. When reducing the diffraction grating pitches from 512 to 16 pixels, the diffraction efficiency stays at its maximum level. For grating pitches as small as two pixels, i.e. only one pixel switches surrounded by two unswitched pixels (or four for the “checkerboard” grating), the diffraction efficiency is about 0.85 of the maximum level.

Funding. UK Engineering and Physical Sciences Research Council (EPSRC) through the EPSRC Centre for Doctoral Training in Integrated Photonic and Electronic Systems (EP/L015455/1).

Acknowledgments. The authors would like to thank Jasper Display Corp. for the help on the operation of their LOCS backplanes.

Disclosures. The authors declare no conflicts of interest.

Data availability. Data underlying the results presented in this paper are not publicly available at this time but may be obtained from the authors upon reasonable request.

References

1. T. Kozacki and M. Chlipala, "Color holographic display with white light LED source and single phase only SLM," Opt. Express **24**(3), 2189-2199 (2016).
2. K. Wakunami, P. Y. Hsieh, R. Oi, T. Senoh, H. Sasaki, Y. Ichihashi, M. Okui, Y. P. Huang, and K. Yamamoto, "Projection-type see-through holographic three-dimensional display," Nat. Commun. **7**, 1–7 (2016).
3. A. Maimone, A. Georgiou, and J. S. Kollin, "Holographic near-eye displays for virtual and augmented reality," ACM Trans. Graph. **36**(4), 1–16 (2017).
4. N. Matsuda, A. Fix, and D. Lanman, "Focal surface displays," ACM Trans. Graph. **36**(4), 1–14 (2017).
5. J. Christmas, D. Masiyano, and N. Collings, "Holographic Automotive Head Up Displays," Electron. Displays 2015 (March), 1–8 (2015).
6. A. O. Yontem, K. Li, D. Chu, V. Meijering, and L. Skrypchuk, "Prospective immersive human-machine interface for future vehicles: multiple zones turn the full windscreen into a head-up display", IEEE Vehicular Technology Mag. **16**(1), 83–92 (2021).
7. Spatial Light Modulator Market by Application, Resolution, Type and Geography - Global Forecast to 2020 (2016), http://marketsandmarkets.com.
8. I. Ouadghiri-Idrissi, R. Giust, L. Froehly, M. Jacquot, L. Furfaro, J. M. Dudley, and F. Courvoisier, "Arbitrary shaping of on-axis amplitude of femtosecond Bessel beams with a single phase-only spatial light modulator," Opt. Express **24**(11), 11495-11504 (2016).
9. T. F. Dixon, L. W. Russell, A. Andres-Arroyo, and P. J. Reece, "Using back focal plane interferometry to probe the influence of Zernike aberrations in optical tweezers," Opt. Lett. **42**(15), 2968-2971 (2017).
10. G. Pesce, G. Volpe, O. M. Marago, P. H. Jones, S. Gigain, A. Sasso, and G. Volpe, "A Step-by-step Guide to the Realisation of Advanced Optical Tweezers," J. Opt. Soc. Am. B **32**(5), 84–98 (2015).
11. M. Wang, L. Zong, L. Mao, A. Marquez, Y. Ye, H. Zhao, and F. Vaquero Caballero, "LCOS SLM Study and Its Application in Wavelength Selective Switch," Photonics **4**(2), 22 (2017).
12. H. Yang, B. Robertson, P. Wilkinson, and D. Chu, "Small phase pattern 2D beam steering and a single LCOS design of 40 1 × 12 stacked wavelength selective switches," Opt. Express **24**(11), 12240-12253 (2016).
13. H. Yang, P. Dolan, B. Robertson, P. Wilkinson, and D. Chu, "Crosstalk Spectrum Optimisation for Stacked Wavelength Selective Switches Based on 2D Beam Steering," in *Optical Fiber Communication Conference* (OSA, 2018), pp. 4–6.
14. B. Robertson, H. Yang, M. M. Redmond, N. Collings, J. R. Moore, J. Liu, A. M. Jeziorska-Chapman, M. Pivnenko, S. Lee, A. Wonfor, I. H. White, W. A. Crossland, and D. P. Chu, "Wavelength Selective Switch," J. Light. Technol. **32**(3), 402–410 (2014).
15. J.-Y. Son, B.-R. Lee, O. O. Chernyshov, K.-A. Moon, and H. Lee, "Holographic display based on a spatial DMD array.," Opt. Lett. **38**(16), 3173–3176 (2013).
16. P. F. Van Kessel, L. J. Hornbeck, R. E. Meier, and M. R. Douglass, "A MEMS-based projection display," Proc. IEEE **86**(8), 1687–1704 (1998).
17. Y. Pan, J. Liu, X. Li, and Y. Wang, "A Review of Dynamic Holographic Three-Dimensional Display: Algorithms, Devices, and Systems," IEEE Trans. Ind. Informatics **12**(4), 1599–1610 (2016).
18. X. Wang, H. Dai, and K. Xu, "Tunable reflective lens array based on liquid crystal on silicon.," Opt. Express **13**(2), 352–357 (2005).
19. N. Collings, T. Davey, J. Christmas, D. Chu, and B. Crossland, "The Applications and Technology of Phase-Only Liquid Crystal on Silicon Devices," IEEE J. Disp. Technol. **7**(3), 112–119 (2011).
20. N. Collings, J. L. Christmas, D. Masiyano, and W. A. Crossland, "Real-time phase-only spatial light modulators for 2D holographic display," J. Disp. Technol. **11**(3), 1–7 (2015).
21. A. Forbes, A. Dudley, and M. McLaren, "Creation and detection of optical modes with spatial light modulators," Adv. Opt. Photonics **8**(2), 200-227 (2016).
22. Z. Zhang, Z. You, and D. Chu, "Fundamentals of phase-only liquid crystal on silicon (LCOS) devices," Light Sci. Appl. **3**(10), 1–10 (2014).
23. E. Moon, M. Kim, J. Roh, H. Kim, and J. Hahn, "Holographic head-mounted display with RGB light emitting diode light source," Opt. Express **22**(6), 6526-6534 (2014).
24. Z. Luo, F. Peng, H. Chen, M. Hu, J. Li, Z. An, and S.-T. Wu, "Fast-response liquid crystals for high image quality wearable displays," Opt. Mater. Express **5**(3), 603-610 (2015).
25. J. Li, Q. Smithwick, and D. Chu, "Full bandwidth dynamic coarse integral holographic displays with large field of view using a large resonant scanner and a galvanometer scanner," Opt. Express **26**(13), 17459–17476 (2018).
26. D. Chu, "Video-rate holograms power up", Nature Electronics 1(4), 214-215 (2018).
27. J. Chu, D. Chu, and Q. Smithwick, "Encoding and multiplexing of 2D images with orbital angular momentum beams and the use of multiview color displays", Research 2019, 9564593 (2019).
28. F. Gou, H. Chen, M.-C. Li, S.-L. Lee, and S.-T. Wu, "Submillisecond-response liquid crystal for high-resolution virtual reality displays.," Opt. Express **25**(7), 7984–7997 (2017).
29. Y. Huang, H. Chen, G. Tan, H. Tobata, S. Yamamoto, E. Okabe, Y.-F. Lan, C.-Y. Tsai, and S.-T. Wu, "Optimized blue-phase liquid crystal for field-sequential-color displays," Opt. Mater. Express **7**(2), 641–650 (2017).
30. S. He, J. H. Lee, H. C. Cheng, J. Yan, and S. T. Wu, "Fast-response blue-phase liquid crystal for color-sequential projection displays," IEEE/OSA J. Disp. Technol. **8**(6), 352–356 (2012).

31. X. Li, C. P. Chen, Y. Li, P. Zhou, X. Jiang, N. Rong, S. Liu, G. He, J. Lu, and Y. Su, "High-Efficiency Video-Rate Holographic Display Using Quantum Dot Doped Liquid Crystal," J. Disp. Technol. **12**(4), 362–367 (2016).
32. W. Duan, P. Chen, B.-Y. Wei, S.-J. Ge, X. Liang, W. Hu, and Y.-Q. Lu, "Fast-response and high-efficiency optical switch based on dual-frequency liquid crystal polarization grating," Opt. Mater. Express **6**(2), 597-602 (2016).
33. J. F. Algorri, N. Bennis, J. Herman, P. Kula, V. Urruchi, and J. M. Sánchez-Pena, "Low aberration and fast switching microlenses based on a novel liquid crystal mixture," Opt. Express **25**(13), 14795–14808 (2017).
34. Y.-H. Lee, F. Gou, F. Peng, and S.-T. Wu, "Hysteresis-free and submillisecond-response polymer network liquid crystal," Opt. Express **24**(13), 14793-14800 (2016).
35. F. Peng, Y. Huang, F. Gou, M. Hu, J. Li, Z. An, and S.-T. Wu, "High performance liquid crystals for vehicle displays," Opt. Mater. Express **6**(3), 717-726 (2016).
36. E. Nowinowski-Kruszelnicki, J. Kedzierski, Z. Raszewski, L. Jaroszewicz, R. Dabrowski, M. Kojdecki, W. Piecek, P. Perkowski, K. Garbat, M. Olifierczuk, M. Sutkowski, K. Ogrodnik, P. Morawiak, and E. Miszczyk, "High birefringence liquid crystal mixtures for electro-optical devices," Opt. Appl. **42**(1), 167–180 (2012).
37. Y. H. Fan, Y. H. Lin, H. Ren, S. Gauza, and S. T. Wu, "Fast-response and scattering-free polymer network liquid crystals for infrared light modulators," Appl. Phys. Lett. **84**(8), 1233–1235 (2004).
38. F. Peng, H. Chen, S. Tripathi, R. J. Twieg, and S.-T. Wu, "Fast-response infrared phase modulator based on polymer network liquid crystal," Opt. Mater. Express **5**(2), 265-273 (2015).
39. J. Sun, S.-T. Wu, and Y. Haseba, "A low voltage submillisecond-response polymer network liquid crystal spatial light modulator," Appl. Phys. Lett. **104**(2), 023305 (2014).
40. R. M. Hyman, A. Lorenz, and T. D. Wilkinson, "Phase modulation using different orientations of a chiral nematic in liquid crystal over silicon devices," Liq. Cryst. **43**(1), 83–90 (2016).
41. H. Kikuchi, M. Yokota, Y. Hisakado, H. Yang, and T. Kajiyama, "Polymer-stabilized liquid crystal blue phases," Nat. Mater. **1**(1), 64–68 (2002).
42. R. M. Hyman, A. Lorenz, S. M. Morris, and T. D. Wilkinson, "Polarization-independent phase modulation using a blue-phase liquid crystal over silicon device," Appl. Opt. **53**(29), 6925-6929 (2014).
43. W. J. Hossack, E. Theofanidou, J. Crain, K. Heggarty, and M. Birch, "High-speed holographic optical tweezers using a ferroelectric liquid crystal microdisplay," Opt. Express **11**(17), 2053-2059 (2003).
44. N. A. Clark and S. T. Lagerwall, "Submicrosecond bistable electro-optic switching in liquid crystals," Appl. Phys. Lett. **36**(11), 899–901 (1980).
45. E. Buckley, "Holographic laser projection," IEEE/OSA J. Disp. Technol. **7**(3), 135–140 (2011).
46. Y. Tong, M. Pivnenko, and D. Chu, “Improvements of phase linearity and phase flicker of phase-only LCoS devices for holographic applications”, Appl. Optics 58(34), G248-G255 (2019).
47. Y. Tong, M. Pivnenko, and D. Chu “Implementation of 10-Bit Phase Modulation for Phase-Only LCOS Devices Using Deep Learning”, Adv. Devices & Instrumentation 2020, 9515747 (2020).
48. Y. Huang, Z. He, and S.-T. Wu, "Fast-response liquid crystal phase modulators for augmented reality displays," Opt. Express **25**(26), 32757-32766 (2017).
49. T. X. Lu, M. Pivnenko, B. Robertson, and D. P. Chu, “Pixel-level fringing-effect model to describe the phase profile and diffraction efficiency of a liquid crystal on silicon device”, Appl. Optics **54**(9), 5903-5910 (2015).
50. J. Li, S. Brugioni, R. Meucci, S. Faetti and S.T. Wu, “Infrared refractive indices of liquid crystals,” J. Appl. Phys., **97**(7), 073501 (2005).
51. Z. Zhang, A. M. Jeziorska-Chapman, N. Collings, M. Pivnenko, J. Moore, B. Crossland, D. Chu, and B. Milne, "High Quality Assembly of Phase-Only Liquid Crystal on Silicon (LCOS) Devices," J. Disp. Technol. **7**(3), 120–126 (2011).